Transportation Engineering 14 (2023) 100208

Contents lists available at ScienceDirect

Transportation Engineering

journal homepage: www.sciencedirect.com/journal/transportation-engineering

Full Length Article

Macroscopic traffic characterization based on driver memory and traffic stimuli

Zawar H. Khan [b], Waheed Imran [a,*], T. Aaron Gulliver [b], Khurram S. Khattak [d], Ghayas Ud Din [c], Nasru Minallah [d], Mushtaq A. Khan [e]

[a] Department of Civil, Environmental and Architectural Engineering, University of Naples, Federico II, Via Claudio 21, Naples, 80125, Italy
[b] Department of Electrical and Computer Engineering, University of Victoria, PO Box 1700, STN CSC, Victoria, BC Canada V8W 2Y2 Canada
[c] National Institute of Urban Infrastructure Planning, University of Engineering and Technology, Peshawar, 25000, Pakistan
[d] Department of Computer System Engineering, University of Engineering and Technology, Peshawar, 25000, Pakistan
[e] Department of Electrical Engineering, University of Engineering and Technology, Mardan, Pakistan

ARTICLE INFO

Keywords:
Macroscopic traffic flow
Driver reaction
Distance headway
Driver memory
Zhang model
Flow stability
Numerical stability

ABSTRACT

A new macroscopic traffic flow model is proposed which incorporates traffic alignment behavior at transitions. In this model, velocity is a function of the distance headway and driver response time. It can be used to characterize the traffic flow for both uniform and non uniform headways. The well-known Zhang model characterizes this flow based on driver memory which can produce unrealistic results. The performance of the proposed Khan-Imran-Gulliver (KIG) and Zhang models is evaluated for an inactive bottleneck on a 2000 m circular road. The results obtained show that the traffic behavior with the KIG model is more realistic.

1. Introduction

Traffic models play a vital role in the development of strategies to mitigate congestion [1,2]. Vehicle dynamics are based on the distance between vehicles (distance headway), driver reaction to a stimuli [3], velocity differences, road pavement condition, and driving environment. A small headway results in quick driver reaction which can produce large changes in traffic. An aggressive driver will typically maintain a small headway while a sluggish driver will have a large headway. With a large headway, driver reaction is slow and smooth changes in flow occur. Aggressive drivers are a major cause of traffic accidents. It has been stated that 55.7% of traffic fatalities are caused by these drivers [4]. Aggressive driving behavior can increase fuel consumption and carbon monoxide emissions [5]. Further, it has been observed that 25% of all road accidents are rear-end collisions. One of the major factors contributing to these collisions is distance headway (rearward). If this headway is less than the required safe headway, drivers will not have enough time to safely react to sudden braking by leading vehicles [6,7]. Thus, the distance headway and driver reaction should be incorporated in traffic models to characterize traffic flow dynamics.

Macroscopic models characterize the aggregate behavior of traffic and are widely employed because they are simple to implement and have low computational complexity [8,9]. The Lighthill, Whitham and Richards (LWR) model was the first to be developed and can be expressed as [10,11]

$$\rho_t + (\rho v(\rho))_x = 0, \tag{1}$$

where v is speed, ρ is density, and $v(\rho)$ is the relationship between speed and density under equilibrium traffic conditions. This model is based on traffic continuum such that the law of mass conservation is obeyed. Further, traffic changes are assumed to be small and occur instantaneously, which correspond to ideal conditions on a long road. Thus, this model cannot accurately characterize large changes such as with stop and go traffic [12], and sudden changes in velocity [13–15].

In [16], an acceleration term was added to improve the LWR model. Payne proposed a second order model which incorporates traffic adjustments based on driver response (anticipation) [17,18]. This model characterizes driver reaction to a forward stimuli [15], and changes in velocity are based on a relaxation term. Whitham introduced a similar model which is known as the Payne Whitham (PW) model. This model assumes vehicles have uniform behavior [19], but in reality this is not

* Corresponding author.
E-mail address: waheed.imran@unina.it (W. Imran).

https://doi.org/10.1016/j.treng.2023.100208
Received 30 June 2023; Received in revised form 25 September 2023; Accepted 12 October 2023
Available online 14 October 2023

true. As a consequence, the PW model can produce unsatisfactory results [18].

The PW model was improved in [20] by considering the anticipation and reaction times for small changes in velocity and density. In [21], the relaxation time τ was assumed to be a function of the density. It was shown in [13] that forward conditions influence the traffic flow and changes in velocity should not be greater than the average velocity. Further, traffic is affected by forward vehicles, and this is ignored in the PW model. This can result in negative speeds with a large traffic flow, which is impossible [22,23]. However, speed differences in the lanes of multilane roads allow vehicles to travel faster then the average speed [24]. The PW model was modified in [25] so that velocity changes are below the average speed. However, the results can be unrealistic when the density is high [26].

Zhang [18] improved the PW model by considering both density and velocity (speed). However, the density is adjusted instantaneously so the time taken by a driver to align to a forward stimulus is ignored. This model incorporates microscopic car-following and macroscopic fluid-like traffic flow behavior [27], but driver response based on distance headway is not considered which can lead to unrealistic results.

The PW model was improved in [28] by considering harmonization during transitions. This model incorporates the forward and lateral distances between vehicles, reaction and harmonization times, and changes in velocity. The equilibrium velocity distribution is characterized based on the density and travel time of real non-homogeneous traffic. In [29], a macroscopic model for traffic flow in the presence of Connected and Autonomous Vehicles (CAVs) was proposed. The anticipation behavior of CAVs is modeled based on the reaction times of CAVs and distances between vehicles. However, this model is based on speed and not density.

Second order models have been employed in a number of applications. In [30], a model was proposed which considers graded highways and roads in hilly regions. This type of terrain presents difficulties for drivers due to the limited visibility which impairs their ability to properly assess the speed of approaching cars. A new macroscopic traffic flow model was presented in [31] which incorporates driver anticipation and the links between micro and macro factors. Recent research has concentrated on factors such as forward and backward anticipation, but these factors have not been considered together. This is crucial for accurate modeling of graded highways and determining traffic flows.

In real traffic, drivers typically observe following cars via the rear view mirror. This information is important to properly respond to changes in traffic and ensure a safe and stable traffic flow. The rapid development of urban transportation systems coupled with modern information technology has led to Intelligent Transportation Systems (ITS) which can provide drivers with detailed traffic information. This motivated development of the Backward Looking Optimal Velocity (BLOV) model [32]. This model was used to demonstrate that backward information affects congestion. ITS information was considered in [33] along with anticipation and backward observations. It was shown that anticipation and backward observations can improve traffic stability. These observations were considered in the lattice hydrodynamic model [34] and in [35,36]. However, only microscopic models have been developed and none of the existing macroscopic models incorporate backward observations.

In this paper, a macroscopic traffic model is developed based on driver response to a traffic stimuli and the rearward and forward distance headways to incorporate the effects of anticipation and backward observations. Vehicle alignment to a forward stimulus influences this distance. A sluggish driver has a large distance headway with forward vehicles and a small headway with rearward vehicles, and the response to forward vehicles is slow. Conversely, an aggressive driver has a small distance headway with forward vehicles and a large headway with rearward vehicles. A typical driver falls between these two cases. The changes in traffic flow with a typical driver are smaller than with a sluggish driver. Thus, spatial changes in density and velocity in the KIG model are based on driver behavior. For more realistic traffic evolution, the rearward distance headway is included. The performance of the KIG model is compared with the Zhang model for a 2000 m circular road with an inactive bottleneck. The results obtained show that the KIG model can characterize traffic behavior more realistically because it incorporates driver behavior and physical road characteristics.

The remainder of this paper is organized as follows. The KIG model is presented in Section 2 and the hyperbolicity is investigated in Section 3. Section 4 examines the flow and numerical stability. The performance of the KIG and Zhang models is investigated in Section V, and finally some conclusions are given in Section 5.

2. Traffic flow modeling

Zhang [18] developed a model based on changes in the equilibrium velocity distribution. According to this model, traffic density changes are proportional to the changes in velocity during alignment. The driver response of this model is $\rho v^{'}(\rho)$. Since the equilibrium velocity distribution is a monotonically decreasing function of density, this response is inversely proportional to the density. Zhang [27] developed a second model that also considers driver resistance to changes in velocity. It includes the response due to the distance headway with a forward vehicle [8]. This model can be expressed as

$$\rho_t + (\rho v)_x = 0, \tag{2}$$

$$v_t + (v + 2\beta c(\rho))v_x + \frac{c^2(\rho)}{\rho}\rho_x = \frac{v(\rho) - v}{\tau} + \mu(\rho)v_{xx}, \tag{3}$$

where $\frac{(v(\rho)-v)}{\tau}$ is the relaxation term which determines velocity alignment during the relaxation time τ at traffic changes (transitions) [37], $c(\rho) = \rho v(\rho)^{'}$ is the driver response, v_{xx} is the second derivative of velocity with respect to space, β is a dimensionless parameter which corresponds to driver memory [27], and $\mu(\rho) = 2\beta\tau c^2(\rho)$. The term $\mu(\rho)$ indicates that driver resistance to changes in velocity is a function of driver memory β. For negligible changes in traffic, $\beta = 0$, which implies that $v^{'}(\rho) = 0$ as the density is low. Further, there is no driver memory in this case as changes in flow are small. β is large for a high density as large changes in flow occur.

The Zhang model has been shown to produce unstable traffic behavior when $0 < \beta << 1$ and $\beta >> 1$ [27]. The term $\frac{c^2(\rho)}{\rho}\rho_x$ is the spatial presumption of a driver [38] which indicates that spatial traffic evolution is based on driver behavior. The viscosity term $\mu(\rho)v_{xx}$ smooths out large traffic changes and ensures that the density and velocity are stable and stay within range. However, this term has no physical meaning so the results may not be realistic.

Second order traffic models with no viscosity term are known as inviscid models [27]. Setting the viscosity term in the Zhang model to 0 gives

$$\rho_t + (\rho v)_x = 0, \tag{4}$$

$$v_t + (v - 2\beta|c(\rho)|)v_x + \frac{c^2(\rho)}{\rho}\rho_x = \frac{v(\rho) - v}{\tau}. \tag{5}$$

Driver memory is characterized by a constant β in this model. Further, spatial changes in traffic are based on the term $\rho v^{'}(\rho)$ so driver presumption is a function of the density dependent velocity profile. This can result in excessive changes in traffic when the density is large. For a more realistic characterization, both driver memory and $\rho v^{'}(\rho)$ should be a function of driver response.

During the reaction time, a driver perceives forward stimuli and reacts to align to the conditions ahead. An aggressive driver reacts quickly and so takes less time to respond than a typical driver while a sluggish driver responds slowly [1]. In this paper, driver memory is

defined as the ratio of reaction time τ_r to relaxation time τ

$$\beta = \frac{\tau_r}{\tau}. \tag{6}$$

Then $\beta = 1$ for a typical driver, $\beta < 1$ for an aggressive driver, and $\beta > 1$ for a slow driver.

Spatial traffic alignment is influenced by the presence of vehicles in the vicinity [27]. A stimulus for a driver is the distance headway between vehicles. With an aggressive driver, there is a large rearward distance headway and with a slow driver, this headway is small. The forward distance headway maintained between vehicles is h_f and the reaction of a driver to this headway is β. Thus, the driver response to forward vehicles can be characterized as [27]

$$\beta \times h_f. \tag{7}$$

The rearward distance headway maintained between vehicles is h_r. Changes in τ_r are a function of the relaxation time so the reaction of a driver to the rearward distance headway based on memory can be expressed as $a - \beta$ where $0 < \beta \leq a$. Then the driver response to rearward vehicles can be characterized as [27]

$$(a-\beta)h_r. \tag{8}$$

The driver response from (7) and (8) is

$$\beta h_f + (a-\beta)h_r \tag{9}$$

For a typical driver, $\beta = 1$ so $\tau_r = \tau$ and $h_f = h_r$. For an aggressive driver, $\beta < 1$ so $\tau_r < \tau$. In this case, the forward distance headway is smaller than with a typical driver and the rearward distance headway is larger. For a sluggish driver, $\beta > 1$ so that $\tau_r > \tau$. Then the forward distance headway is larger than with a typical driver and the rearward distance headway is smaller.

The velocity is given by

$$v = \frac{s}{\tau}, \tag{10}$$

where s is the distance covered during time τ. The velocity based on forward and rearward vehicles from (9) and (10) is

$$\frac{\beta h_f + (a-\beta)h_r}{\tau}. \tag{11}$$

In (5), $c(\rho)$ is the rate at which changes in traffic propagate during alignment. However, these changes are affected by the driver response. From (11), driver presumption of changes in density can be expressed as

$$c(\rho) = \left(\frac{\beta h_f + (a-\beta)h_r}{\tau}\right). \tag{12}$$

Thus for the KIG model, the acceleration relationship based on driver response from (5) and (12) is

$$v_t + \left(v - \frac{(\beta h_f + (a-\beta)h_r)\tau_r}{\tau^2}\right)v_x + \frac{\left(\frac{(\beta h_f + (a-\beta)h_r)}{\tau}\right)^2}{\rho}\rho_x = \frac{v(\rho)-v}{\tau}. \tag{13}$$

According to (13), a driver aligns to forward conditions based on stimuli (distance headway) and memory (response time). Unlike the Zhang model (3), there is no viscosity term to smooth large traffic changes in traffic. Note that the first equation of the KIG model is the same as in the Zhang model

$$\rho_t + (\rho v)_x = 0. \tag{14}$$

3. Model hyperbolicity

A second order traffic system must be hyperbolic such that the upstream rate of change during congestion is less than the rate of change in the downstream during free flow [39,40]. Further, hyperbolicity guarantees finite changes in velocity [1]. The conserved form of the KIG model from (13) and (14) is

$$\begin{pmatrix}\rho\\ v\end{pmatrix}_t + \begin{pmatrix} v & \rho \\ \dfrac{\left(\frac{(\beta h_f + (a-\beta)h_r)}{\tau}\right)^2}{\rho} & \left(v - \dfrac{(\beta h_f + (a-\beta)h_r)\tau_r}{\tau^2}\right)\end{pmatrix}\begin{pmatrix}\rho\\ v\end{pmatrix}_x = \begin{pmatrix}0\\ \dfrac{v(\rho)-v}{\tau}\end{pmatrix}, \tag{15}$$

and the homogeneous form is

$$\begin{pmatrix}\rho\\ v\end{pmatrix}_t + \begin{pmatrix} v & \rho \\ \dfrac{\left(\frac{(\beta h_f + (a-\beta)h_r)}{\tau}\right)^2}{\rho} & \left(v - \dfrac{(\beta h_f + (a-\beta)h_r)\tau_r}{\tau^2}\right)\end{pmatrix}\begin{pmatrix}\rho\\ v\end{pmatrix}_x = \begin{pmatrix}0\\ 0\end{pmatrix}. \tag{16}$$

From the Jacobian matrix

$$\begin{pmatrix} v & \rho \\ \dfrac{\left(\frac{(\beta h_f + (a-\beta)h_r)}{\tau}\right)^2}{\rho} & \left(v - \dfrac{(\beta h_f + (a-\beta)h_r)\tau_r}{\tau^2}\right)\end{pmatrix},$$

the eigenvalues of the KIG model are

$$\begin{aligned}\lambda_1 &= v - \left(\beta + \sqrt{1+\beta^2}\right)\left(\frac{(\beta h_f + (a-\beta)h_r)}{\tau}\right),\\ \lambda_2 &= v - \left(\beta - \sqrt{1+\beta^2}\right)\left(\frac{(\beta h_f + (a-\beta)h_r)}{\tau}\right).\end{aligned} \tag{17}$$

The KIG model is hyperbolic as the eigenvalues are distinct and real. Further, they indicate that changes in velocity are based on driver behavior. During alignment, forward changes disseminate at a rate λ_2 for a smooth flow while rearward changes disseminate at a rate λ_1 for a congested flow. In the case $h_r = h_f = h$, i.e. when the forward and rearward distance headways are equal, $\tau_r = 0$ so the eignevalues are

$$\lambda_1 = v - a\frac{h}{\tau}, \lambda_2 = v + a\frac{h}{\tau}. \tag{18}$$

From (4) and (5), the Zhang model can be expressed as

$$\begin{pmatrix}\rho\\ v\end{pmatrix}_t + \begin{pmatrix} v & \rho \\ \dfrac{c(\rho)^2}{\rho} & (v - 2\beta|c(\rho)|)\end{pmatrix}\begin{pmatrix}\rho\\ v\end{pmatrix}_x = \begin{pmatrix}0\\ \dfrac{v(\rho)-v}{\tau}\end{pmatrix}, \tag{19}$$

and its homogeneous form is

$$\begin{pmatrix}\rho\\ v\end{pmatrix}_t + \begin{pmatrix} v & \rho \\ \dfrac{c(\rho)^2}{\rho} & (v - 2\beta|c(\rho)|)\end{pmatrix}\begin{pmatrix}\rho\\ v\end{pmatrix}_x = \begin{pmatrix}0\\ 0\end{pmatrix}. \tag{20}$$

From the Jacobian matrix

$$\begin{pmatrix} v & \rho \\ \dfrac{c(\rho)^2}{\rho} & (v - 2\beta|c(\rho)|)\end{pmatrix},$$

the eigenvalues are

$$\lambda_1 = v - \left(\beta + \sqrt{1+\beta^2}\right)|c(\rho)|, \lambda_2 = v - \left(\beta - \sqrt{1+\beta^2}\right)|c(\rho)|. \tag{21}$$

Thus, traffic changes in the forward and rearward directions are based on driver memory and changes in the equilibrium velocity distribution. With no driver memory ($\beta = 0$)

$$\lambda_1 = v - |c(\rho)|, \lambda_2 = v + |c(\rho)|, \tag{22}$$

so $c(\rho)$ determines the changes in traffic. Thus, with the Zhang model these changes are based on constant driver memory and driver behavior during alignment is ignored.

4. Traffic flow stability

In this section, the stability of the Zhang and KIG models is examined. It is assumed that the initial density distribution ρ_0 at $t = 0$ is stable and the initial velocity distribution v_0 is density dependent, i.e. $v_0 = v(\rho_0)$ [41–43]. Changes in velocity and density can be expressed as

$$\begin{aligned} \Delta v &= v - v_0, \\ \Delta \rho &= \rho - \rho_0. \end{aligned} \tag{23}$$

These changes are considered to be periodic functions of $k(x)$ so that [41]

$$\begin{aligned} \Delta v &= v_0 e^{i k(x) + w(t)}, \\ \Delta \rho &= \rho_0 e^{i k(x) + w(t)}, \end{aligned} \tag{24}$$

where $i = \sqrt{-1}$. Thus, the changes in velocity and density over time are $v_0 e^{w(t)}$ and $\rho_0 e^{w(t)}$, respectively.

For simplicity, let $A = \left(\frac{(\beta h_f + (a-\beta)h_r)\tau_r}{\tau^2}\right)$ and $B = \left(\frac{(a-\beta)h_r + \beta h_f}{\tau}\right)^2$ in the KIG model. Substituting (23) in (13) and (14) gives

$$\frac{\partial \Delta\rho}{\partial t} + v\frac{\partial \Delta\rho}{\partial x} + \rho\frac{\partial \Delta v}{\partial x} = 0, \tag{25}$$

$$\frac{\partial \Delta v}{\partial t} = \left(-(v - A)\frac{\partial \Delta v}{\partial x} - \frac{B}{\rho}\frac{\partial \Delta\rho}{\partial x} + \left(\frac{v(\rho) - v}{\tau}\right)\right). \tag{26}$$

During traffic alignment, the temporal and spatial changes in velocity and density from (24) can be expressed as

$$\begin{aligned} \frac{\partial \Delta v}{\partial t} &= w(t) v_0 e^{(i k(x) + w(t))} \\ \frac{\partial \Delta v}{\partial x} &= i k(x) v_0 e^{(i k(x) + w(t))}, \\ \frac{\partial \Delta \rho}{\partial t} &= w(t) \rho_0 e^{(i k(x) + w(t))} \\ \frac{\partial \Delta \rho}{\partial x} &= i k(x) \rho_0 e^{(i k(x) + w(t))}. \end{aligned} \tag{27}$$

For simplicity, denote $k(x)$, and $w(t)$ by k, and w, respectively. Substituting (27) in (25) and (26) [44] gives

$$J\begin{pmatrix} \Delta\rho \\ \Delta v \end{pmatrix} = \begin{pmatrix} 0 \\ 0 \end{pmatrix}, \tag{28}$$

where

$$\begin{aligned} J &= \begin{pmatrix} j_{11} & j_{12} \\ j_{21} & j_{22} \end{pmatrix} \\ &= \begin{pmatrix} (ikv_0 + w) & ik\rho_0 \\ -\frac{ikB}{\rho_0} + \frac{v(\rho_0)'}{\tau} & -w - ik(v_0 - A) - \frac{1}{\tau} \end{pmatrix}, \end{aligned} \tag{29}$$

so that

$$\begin{pmatrix} (ikv_0 + w) & ik\rho_0 \\ -\frac{ikB}{\rho_0} + \frac{v(\rho_0)'}{\tau} & -w - ik(v_0 - A) - \frac{1}{\tau} \end{pmatrix} \begin{pmatrix} \rho_0 e^{(ik+w)} \\ v_0 e^{(ik+w)} \end{pmatrix} = \begin{pmatrix} 0 \\ 0 \end{pmatrix}. \tag{30}$$

It is assumed that $\begin{pmatrix} \Delta\rho \\ \Delta v \end{pmatrix}$ is the solution for the KIG model such that the temporal and spatial changes in traffic are small, i.e. the changes in velocity and density are small.

With a stable system, the effect of traffic changes decrease over time so that $\det(J) = 0$ [45]. From (30), we then have

$$\begin{aligned} w^2 + \left(\frac{1}{\tau} - ikA + i2kv_0\right)w - k^2v_0^2 + k^2v_0A + k^2B \\ + i\frac{kv_0 + k\rho_0 v(\rho_0)'}{\tau} = 0, \end{aligned} \tag{31}$$

which gives

$$w^2 + (\phi_1 + i\epsilon_1)w + \phi_2 + i\epsilon_2 = 0, \tag{32}$$

where

$$\phi_1 = \frac{1}{\tau},$$

$$\epsilon_1 = -kA + 2kv_0,$$

$$\phi_2 = -k^2v_0^2 + k^2v_0A + k^2B,$$

and

$$\epsilon_2 = \frac{kv_0 + k\rho_0 v(\rho_0)'}{\tau}.$$

The solutions of (32) are

$$w_\pm = \frac{-(\phi_1 + i\epsilon_1) \pm \sqrt{(\phi_1 + i\epsilon_1)^2 - 4(\phi_2 + i\epsilon_2)}}{2}. \tag{33}$$

Traffic is stable if $\mathrm{Re}(w_+) \le 0$. The term $(\phi_1 + i\epsilon_1)^2 - 4(\phi_2 + i\epsilon_2)$ under the radical sign in (33) is

$$\sqrt{R \pm I} = \sqrt{\frac{\left(\sqrt{R^2 + I^2} + R\right)}{2}} \pm i\sqrt{\frac{\left(\sqrt{R^2 + I^2} - R\right)}{2}}, \tag{34}$$

so that

$$\mathrm{Re}\left(\sqrt{\frac{(\phi_1 + i\epsilon_1)^2}{4} - (\phi_2 + i\epsilon_2)}\right) = \sqrt{\frac{\left(\sqrt{R^2 + I^2} + R\right)}{2}}, \tag{35}$$

where $I = \frac{(\phi_1\epsilon_1 - 2\phi_2)}{2}$ and $R = \frac{(\phi_1^2 - \epsilon_1^2 - 4\phi_2)}{4}$ [46]. The real part of (33) is

$$\mathrm{Re}(w_\pm) = -\frac{\phi_1}{2} \pm \sqrt{\frac{\left(\sqrt{R^2 + I^2} + R\right)}{2}}. \tag{36}$$

Traffic is unstable if $\mathrm{Re}(w_+)$ is positive which occurs when

$$-\frac{\phi_1}{2} + \sqrt{\frac{1}{2}(\sqrt{R^2 + I^2} + R)} > 0, \tag{37}$$

which gives

$$R^2 + I^2 > \frac{\phi_1^2}{4} + R^2 - \phi_1^2 R, \tag{38}$$

or

$$\phi_1^2 R + I^2 > \frac{\phi_1^4}{4}. \tag{39}$$

Substituting the values for I and R gives

$$\phi_1^2\phi_2 - \epsilon_2^2 + \phi_1\epsilon_1\epsilon_2 > 0, \tag{40}$$

and then substituting ϕ_1, ϕ_2, ϵ_1, and ϵ_1, the instability condition is obtained as

$$\rho_0^2 v'(\rho_0)^2 + A\rho_0 v'(\rho_0) - B > 0. \tag{41}$$

Using $A = 2\tau_r\left(\frac{(2-\beta)h_r+\beta h_f}{\tau^2}\right)$ and $B = \left(\frac{(2-\beta)h_r+\beta h_f}{\tau}\right)^2$, the KIG model is unstable when

$$\rho_0^2 v'(\rho_0)^2 + 2\tau_r\frac{(2-\beta)h_r+\beta h_f}{\tau^2}\rho_0 v'(\rho_0) - \left(\frac{(2-\beta)h_r+\beta h_f}{\tau}\right)^2 > 0. \tag{42}$$

Since equilibrium velocity decreases as the density increases, i.e. $v'(\rho) \le 0$, a stable traffic flow requires that

$$\rho_0|v'(\rho_0)| \le \sqrt{-2\tau_r\frac{(2-\beta)h_r+\beta h_f}{\tau^2}\rho_0 v'(\rho_0) + \left(\frac{(2-\beta)h_r+\beta h_f}{\tau}\right)^2}. \tag{43}$$

We have that

$$v'(\rho_0) = \frac{\partial v(\rho_0)}{\partial \rho_0}, \tag{44}$$

and substituting this in (43) gives

$$\rho_0\left|\frac{\partial v(\rho_0)}{\partial \rho_0}\right| \le \sqrt{-2\tau_r\frac{(2-\beta)h_r+\beta h_f}{\tau^2}\rho_0 v'(\rho_0) + \left(\frac{(2-\beta)h_r+\beta h_f}{\tau}\right)^2}, \tag{45}$$

which indicates that traffic is stable when there are small changes in velocity during alignment. As the density increases, the changes in velocity increase, i.e. $\left|\frac{\partial v(\rho_0)}{\partial \rho_0}\right|$ increases. However, the RHS also increases so the flow remains stable.

For the Zhang model, $A = 2\beta c(\rho_0)$, and $B = c(\rho_0)^2$, so the corresponding stability condition is

$$\rho_0^2 v'(\rho_0)^2 - 2\beta|c(\rho_0)| - (c(\rho_0))^2 > 0. \tag{46}$$

For $v'(\rho_0) \le 0$

$$\rho_0\left|\frac{\partial v(\rho_0)}{\partial \rho_0}\right| \le \sqrt{2\beta|c(\rho_0)| + (c(\rho_0))^2}. \tag{47}$$

In this case, the terms on the RHS are $2\beta|c(\rho_0)|$ and $(c(\rho_0))^2$. β is a constant and so cannot characterize traffic behaviour under different conditions. Further, $c(\rho_0)$ is density dependent and ignores driver reaction time. We have $|c(\rho_0)| = \left|\rho_0\frac{\partial v(\rho_0)}{\partial \rho_0}\right|$ which is an increasing function of density, so an increase in density will also increase the RHS which keeps the flow stable. However, this stability mechanism is not based on real traffic behavior and so is unrealistic.

4.1. Numerical stability

For numerical stability, the convective stability criteria [42] must be satisfied. This requires that the road segment length be greater than the distance covered in a time step. This is known as the Courant-Friedrich-Levy (CFL) condition [47,48] which can be expressed as

$$\frac{\delta t}{\delta x} \times \max|\lambda| \le 1. \tag{48}$$

It is the maximum distance traffic can move in a time step. Thus, to approximate density over this time, the distance covered should be smaller than a road segment so

$$\max|\lambda| \times \delta t \le \delta x, \tag{49}$$

which gives

$$\delta t \le \frac{\delta x}{\max|\lambda|}. \tag{50}$$

The time step δt should satisfy this condition, in which case the slope of the gradient is always less than or equal to 1, which is known as the Courant number given by

$$c = \max|\lambda| \times \frac{\delta t}{\delta x}. \tag{51}$$

The CFL condition $c \le 1$ guarantees numerical stability. For the KIG model, the maximum eigenvalue occurs when traffic has maximum velocity which gives

$$\max|\lambda| = \left|v_m - \left(\beta - \sqrt{1+\beta^2}\right)\left(\frac{(a-\beta)h_r+\beta h_f}{\tau}\right)\right|, \tag{52}$$

and the corresponding stability condition is

$$\delta t < \frac{\delta x}{\max\left|v_m - \left(\beta + \sqrt{1+\beta^2}\right)\left(\frac{(a-\beta)h_r+\beta h_f}{\tau}\right)\right|}. \tag{53}$$

For the Zhang model, the maximum eigenvalue is

$$\max|\lambda| = \left|v - \left(\beta - \sqrt{1+\beta^2}\right)|c(\rho)|\right|, \tag{54}$$

and the corresponding stability condition is

$$\delta t < \frac{\delta x}{\max\left|v - \left(\beta + \sqrt{1+\beta^2}\right)|c(\rho)|\right|}. \tag{55}$$

If (53) and (55) are satisfied, the numerical solutions of the KIG and Zhang models, respectively, will be stable.

5. Performance evaluation

In this section, the KIG and Zhang models are evaluated numerically using the First ORder CEntered (FORCE) scheme [49]. This scheme has been employed previously for second order traffic systems [1,50] as it can be used to approximate abrupt and large changes in traffic flow. It was employed in [51] to estimate pedestrian traffic. Thus, the force scheme can provide accurate numerical results for both pedestrian and vehicular traffic. It is easy to implement and has lower computational complexity than the ROE decomposition scheme [50]. The FORCE scheme combines the first order Lax-Friedrichs and second-order Richtmyer schemes to accurately estimate second order partial differential systems. Nonlinear traffic systems are solved by considering the conservation form which is

$$\Xi_t + f(\Xi)_x = S(\Xi), \tag{56}$$

where Ξ is the vector of data variables, i.e. ρ and v, $f(\Xi)$ is the corresponding vector of functions of the data variables, and $S(\Xi)$ is the vector of source terms [52]. The Zhang model (4) and (5) in conserved form is given by

$$\Xi = \begin{pmatrix} \rho \\ v \end{pmatrix}_t, f(\Xi) = \begin{pmatrix} v & \rho \\ \dfrac{c(\rho)^2}{\rho} & (v - 2\beta|c(\rho)|) \end{pmatrix}_x, \quad S(\Xi) = \begin{pmatrix} 0 \\ \left(\dfrac{v_e(\rho) - v}{\tau}\right) \end{pmatrix}, \tag{57}$$

and the KIG model in conserved form is

$$\Xi = \begin{pmatrix} \rho \\ v \end{pmatrix}_t, f(\Xi) = \begin{pmatrix} v & \rho \\ \dfrac{\left(\frac{\beta h_f + (2-\beta)h_r}{\tau}\right)^2}{\rho} & \left(v - \left(\frac{\left(\beta h_f + (2-\beta)h_r\right)\tau_r}{\tau^2}\right)\right) \end{pmatrix}_x, \quad S(\Xi) = \begin{pmatrix} 0 \\ \left(\dfrac{v_e(\rho) - v}{\tau}\right) \end{pmatrix}. \tag{58}$$

The road length is x_M and there are M equidistant segments so the segment length is $\delta x = x_m/M$. The total time duration is t_N and there are N time steps so a time step is $\delta t = t_N/N$ given by $t_{n+1} - t_n$. At a given time step, Ξ and $f(\Xi)$ are approximated for the road segments $\left(x_i + \frac{\delta x}{2}, x_i - \frac{\delta x}{2}\right)$, and the data variables are obtained for each of the M segments. Let Ξ_i be the average values of the data variables in the ith road segment. Then the traffic flux at the road segment boundaries with the Lax-Friedrichs scheme is

$$\left(f^n_{i+\frac{1}{2}}\left(\Xi^n_i, \Xi^n_{i+1}\right)\right)^l = \frac{1}{2}\left(f\left(\Xi^n_i\right) + f\left(\Xi^n_{i+1}\right)\right) + \frac{1}{2}\frac{\delta t}{\delta x}\left(\Xi^n_i - \Xi^n_{i+1}\right), \tag{59}$$

where $f(\Xi^n_i)$ and $f(\Xi^n_{i+1})$ are the data variable functions in segments i and $i+1$, respectively, and the superscript l denotes the Lax-Friedrich scheme. Using the Richtmyer scheme, the data variables are obtained as

$$\left(\Xi_{i+\frac{1}{2}}\right)^r = \frac{1}{2}\left(\Xi^n_i + \Xi^n_{i+1}\right) + \frac{1}{2}\frac{\delta t}{\delta x}\left(f\left(\Xi^n_i\right) - f\left(\Xi^n_{i+1}\right)\right), \tag{60}$$

where r denotes the Richtmyer scheme. The corresponding traffic flux at the road segment boundaries is

$$\left(f^n_{i+\frac{1}{2}}\left(\Xi^n_i, \Xi^n_{i+1}\right)\right)^r = f\left(\Xi_{i+\frac{1}{2}}\right)^r. \tag{61}$$

Then the flux at the segment boundaries based on the Lax-Friedrichs and Richtmyer schemes is the average of (59) and (61) giving

$$f^{n+1}_i = \frac{1}{2}\left(\left(f^n_{i+\frac{1}{2}}\right)^r + \left(f^n_{i+\frac{1}{2}}\right)^l\right) \tag{62}$$

The updated data variables are obtained by including the source term

$$\Xi^{n+1}_i = \Xi^n_i - \frac{\delta t}{\delta x}\left(f^n_{i+\frac{1}{2}} - f^n_{i-\frac{1}{2}}\right) + \delta t S\left(\Xi^n_i\right). \tag{63}$$

The performance of the KIG and Zhang models is evaluated over a circular road of length 2000 m with periodic boundary conditions. The simulation parameters are given in Table 1. The road and time steps for the KIG and Zhang models are 10 m and 0.01 s, respectively, so that the CFL stability conditions [47] given in (54) and (55) are satisfied. The total simulation time for both models is 10 s. The maximum velocity is 30 m/s and the target is the Greenshields equilibrium velocity distribution [53] which is given by

Table 1
Simulation Parameters.

Parameter	Value
Simulation time	10 s
Length of the circular road	2000 m
Maximum velocity	30 m/s
Time step	0.01 s
Road step	10 m
Reaction time	$\tau_r = 1.5, 2.5, 3.5$ s
Relaxation time	$\tau = 2.5$ s
Headway	$h_r = h_f = 10$ m, 20 m $h_r = 12$ m and $h_f = 15$ m
Driver memory for the KIG model	$\beta = 0.6, 1, 1.4$
Driver memory for the Zhang model	$\beta = 0, 1$
Variation in response time	$a = 2$
Equilibrium velocity distribution	$v(\rho)$ Greenshields
Maximum normalized density	$\rho_m = 1$
Minimum normalized density	$\rho_m = 0$

$$v(\rho) = v_m\left(1 - \frac{\rho}{\rho_m}\right), \tag{64}$$

where $\rho_m = 1$ is the maximum normalized density which means that the road is 100% occupied. This is the most commonly used equilibrium velocity distribution because it has been shown to be appropriate for characterizing traffic flow. It also provides a hyperbolic fundamental flow so the traffic flow increases for a small density and decreases when traffic is congested [54]. This model has been validated using data from Yokohama, Japan, and San Francisco, CA, USA [55–57]

The reaction time is typically in the range $\tau_r = 0.5$ s to 3.5 s, so $\tau_r = 1.5$, 2.5, and 3.5 s are used to evaluate the KIG model. The relaxation time is 2.5 s with $h_f = h_r = 10$ m and 20 m [3,45,58,59], and $h_r = 12$ m and $h_f = 15$ m. The initial density ρ_0 at time $t = 0$ for both the KIG and Zhang models is

$$\rho_0 = \begin{cases} 0.01, & \text{for } x \le 600 \\ 0.8, & \text{for } x \le 1000, \\ 0.01, & \text{for } x \le 1500, \\ 0.8, & \text{for } x \le 2000, \end{cases} \tag{65}$$

over the 2000 m road. Moreover, circular boundary conditions are employed in this study. This simplifies the simulations by eliminating complex boundary conditions, prevents edge effects near boundaries, and approximates real traffic with continuous circulation which is useful for studying steady-state traffic behavior. However, the choice of boundary conditions depends on research objectives and traffic characteristics.

The velocity for the KIG model on a 2000 m circular road at 1 s, 5 s and 10 s with $\tau_r = 1.5$ and $h_f = h_r = 20$ m is shown in Fig. 1. The velocity varies between 6.0 m/s and 29.6 m/s, and is within the limits 0 m/s to 30 m/s. At 1 s, the velocity is 7.8 m/s at 1 m, increases to 29.6 m/s at 280 m and remains at this level until 350 m. It decrease to 6.0 m/s at 810 m, increases to 29.2 m/s at 1270 m, and is 7.8 m/s at 2000 m. At 5 s, the velocity is 11.8 m/s at 1 m, increases to 24.7 m/s at 400 m, decreases to 9.1 m/s at 840 m, and then increases to 22.1 m/s at 1340 m. At 1790 m and 2000 m, the velocity is 7.7 m/s and 11.5 m/s, respectively. At 10 s, the velocity is 13.8 m/s at 1 m and increases to 24.3 m/s at 400 m. It is 13.3 m/s at 890 m, 21.9 m/s at 1390 m, 11.1 m/s at 1820 m, and 13.6 m/s at 2000 m.

The velocity with the KIG model on a 2000 m circular road at 1 s, 5 s, and 10 s with $\tau_r = 2.5$ s and $h = 20$ m is given in Fig. 2. These results show that the velocity becomes smoother over time and changes in velocity decrease. At 1 s, the velocity is 7.4 m/s at 1 m and increases to 29.7 m/s at 350 m. It is approximately 6.1 m/s between 780 m and 880 m, increases to 29.3 m/s at 1270 m, and is approximately 6.1 m/s from 1670 m to 1880 m. The velocity is 7.1 m/s at 2000 m. At 5 s, the velocity

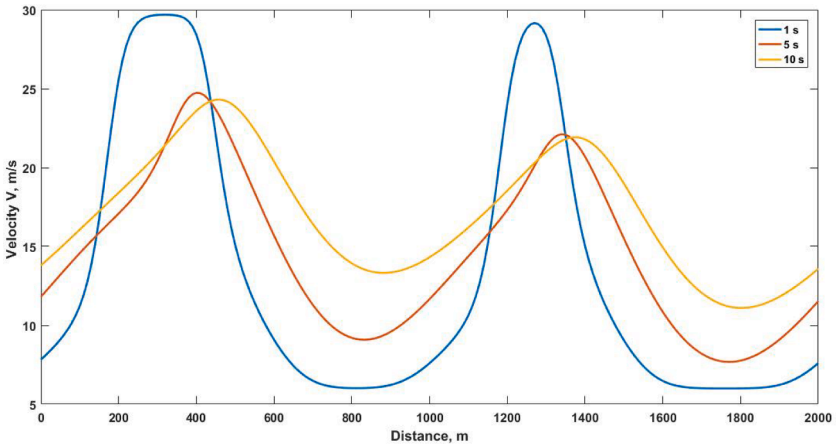

Fig. 1. Velocity with the KIG model on a 2000 m circular road with $h_f = h_r = 20$ m and $\tau_r = 1.5$ s at 1 s, 5 s, and 10 s.

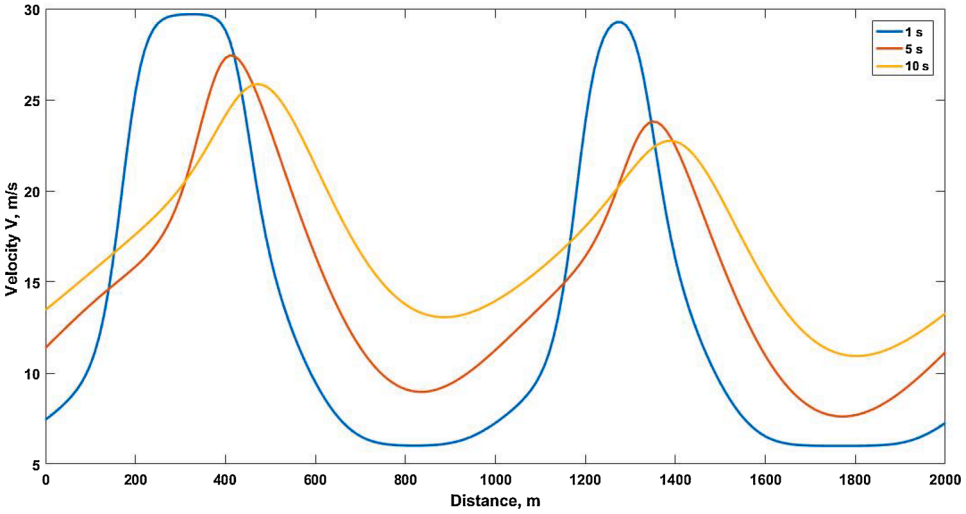

Fig. 2. Velocity with the KIG model on a 2000 m circular road with $h_f = h_r = 20$ m and $\tau_r = 2.5$ s at 1 s, 5 s, and 10 s.

is 11.4 m/s at 1 m, increases to 27.4 m/s at 410 m, decreases to 9.0 m/s at 840 m, and then increases to 23.8 m/s at 1350 m. At 1770 m and 2000 m, the velocity is 7.6 m/s and 11.1 m/s, respectively. At 10 s, the velocity is 13.7 m/s at 1 m and increases to 25.8 m/s at 480 m. It is 13.1 m/s at 890 m, 22.7 m/s at 1380 m, 10.9 m/s at 1810 m, and 13.1 m/s at 2000 m.

The velocity with the KIG model on a 2000 m circular road at 1 s, 5 s, and 10 s with $\tau_r = 3.5$ s and $h_f = h_r = 20$ m is shown in Fig. 3. At 1 s, the

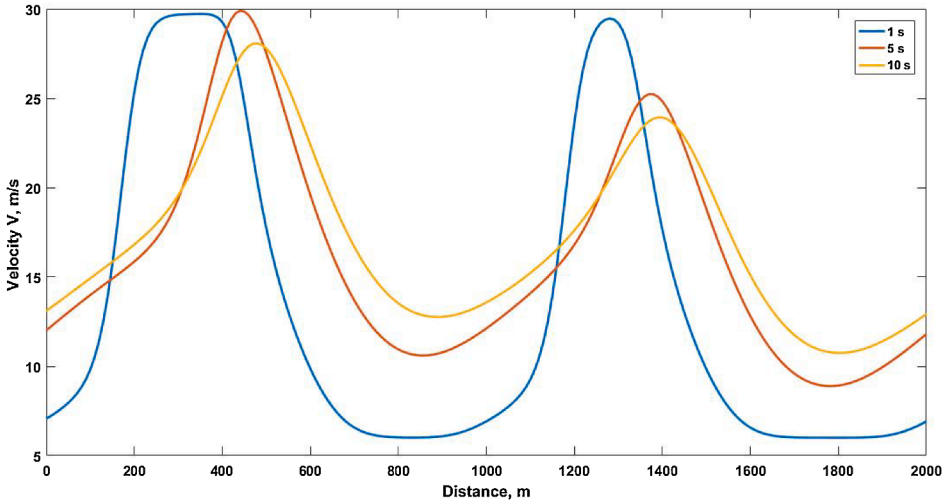

Fig. 3. Velocity with the KIG model on a 2000 m circular road with $h_f = h_r = 20$ m and $\tau_r = 3.5$ s at 1 s, 5 s, and 10 s.

velocity is 7.2 m/s at 1 m, increases to 29.7 m/s at 280 m, and remains at this level until 360 m. It decreases to 6.1 m/s at 890 m, increases to 29.5 m/s at 1280 m, and is approximately 6.0 m/s between 1680 m and 1880 m. The velocity is 6.9 at 2000 m. At 5 s, the velocity is 12.0 m/s at 1 m, increases to 29.9 m/s at 440 m, decreases to 10.6 m/s at 860 m, and then increases to 25.2 m/s at 1380 m. At 1790 m and 2000 m, the velocity is 8.9 m/s and 11.8 m/s, respectively. At 10 s, the velocity is 13.1 m/s at 1 m and increases to 28.1 m/s at 470 m. It is 12.7 m/s at 900 m, 23.9 m/s at 1390 m, 10.7 m/s at 1800 m, and 12.9 m/s at 2000 m.

The velocity with the KIG model on a 2000 m circular road at 10 s with $\tau_r = 1.5$ s, 2.5 s, and 3.5 s, and $h_f = h_r = 10$ m is shown in Fig. 4. With $\tau_r = 1.5$ s, the velocity is 14.3 m/s at 1 m, increases to 23.6 m/s at 440 m, and then decreases to 13.5 m/s at 890 m. The velocity is 21.6 m/s at 1360 m, decreases to 11.2 m/s at 1820 m, and is 13.8 m/s at 2000 m. With $\tau_r = 2.5$ s, the velocity is 14.1 m/s at 1 m, increases to 24.0 m/s at 460 m, and then decreases to 13.4 m/s at 900 m. It is 21.8 m/s at 1370 m, decreases to 11.1 m/s at 1800 m, and is 13.6 m/s at 2000 m. With $\tau_r = 3.5$ s, the velocity is 13.7 m/s at 1 m, increases to 24.6 m/s at 460 m, and then decreases to 13.3 m/s at 880 m. It is 22.1 m/s at 1390 m, decreases to 11.1 m/s at 1810 m, and is 13.5 m/s at 2000 m.

The velocity with the KIG model for 10 s on a 2000 m circular road with $\tau_r = 1.5$ s and $h_f = h_r = 20$ m is shown in Fig. 5. The highest velocity is 29.6 m/s and the lowest is 6.0 m/s, so the velocity is between the maximum 30 m/s and minimum 0 m/s. Further, the velocity becomes smoother over time. The corresponding density is given in Fig. 6. The density also becomes smoother over time and is between the maximum and minimum.

The velocity and density with the KIG model for 10 s on a 2000 m circular road with $\tau_r = 2.5$ s and $h_f = h_r = 20$ m are given in Figs. 7 and 8, respectively. These results show that the density becomes smooth over time and is between the maximum and minimum. The highest velocity is 29.7 m/s while the lowest is 6.0 m/s, so it also stays within range. The velocity becomes smoother over time and the changes are not as large as with $\tau_r = 1.5$ s.

The velocity and density with the KIG model for 10 s on a 2000 m circular road with $\tau_r = 3.5$ s and $h_f = h_r = 20$ m are given in Figs. 9 and 10, respectively. The density is smoother than with $\tau = 1.5$ s and $\tau = 2.5$ s. The velocity stays between the maximum and minimum values as the highest is 29.7 m/s and the lowest is 6.0 m/s.

The velocity with the KIG model on a 2000 m circular road with $\beta = 0.6$, $\tau_r = 1.5$ s, $h_f = 15$ m and $h_r = 12$ m at 1 s, 5 s and 10 s is shown in Fig. 11. At 1 s, the velocity is 8.2 m/s at 1 m and increases to 29.7 m/s at 310 m. It decreases to 6.0 m/s at 800 m, increases to 29.1 m/s at 1270 m, and is approximately 6.0 m/s between 1680 m and 1800 m. The velocity is 8.0 m/s at 2000 m. At 5 s, the velocity is 12.2 m/s at 1 m, increases to 23.0 m/s at 370 m, decreases to 9.2 m/s at 830 m, and then increases to 21.2 m/s at 1310 m. It is 7.7 m/s at 1780 m and 11.9 m/s at 2000 m. At 10 s, the velocity is 14.1 m/s at 1 m, increases to 23.5 m/s at 440 m, decreases to 13.5 m/s at 880 m, and then increases to 21.4 m/s at 1380 m. It is 11.3 m/s at 1800 m and 13.9 m/s at 2000 m.

The velocity with the KIG model on a 2000 m circular road with $\beta = 1$, $\tau_r = 2.5$ s, $h_f = 15$ m and $h_r = 12$ m at 1 s, 5 s, and 10 s is shown in Fig. 12. At 1 s, the velocity is 8.1 m/s at 1 m and is approximately 29.7 m/s between 290 m and 340 m. It decreases to 6.0 m/s at 800 m and remains there until 840 m. The velocity then increases to 29.1 m/s at 1270 m and is approximately 6.1 m/s between 1670 m and 1850 m. It is 7.8 m/s at 2000 m. At 5 s, the velocity is 12.1 m/s at 1 m, increases to 23.5 m/s at 380 m, decreases to 9.2 m/s at 840 m, and then increases to 21.3 m/s at 1320 m. It is 7.7 m/s at 1780 m and 11.8 m/s at 2000 m. At 10 s, the velocity is 14.2 m/s at 1 m, increases to 23.7 m/s at 440 m, decreases to 13.5 m/s at 880 m, and then increases to 21.6 m/s at 1370 m. It is 11.2 m/s at 1810 m and 13.8 m/s at 2000 m.

The velocity with the KIG model on a 2000 m circular road with $\beta = 1.4$, $\tau_r = 3.5$ s, $h_f = 15$ m and $h_r = 12$ m at 1 s, 5 s, and 10 s is shown in Fig. 13. At 1 s, the velocity is 7.9 m/s at 1 m, increases to 29.6 m/s between 300 m and 350 m, and then decreases to 6.1 m/s between 800 m and 870 m. It increases to 29.1 m/s at 1270 m and is approximately 6.1 m/s between 1700 m and 1850 m. The velocity is 7.7 m/s at 2000 m. At 5 s, the velocity is 11.9 m/s at 1 m, increases to 24.2 m/s at 400 m, decreases to 9.1 m/s at 840 m, and then increases to 21.8 m/s at 1330 m. It is 7.7 m/s at 1780 m and 11.6 m/s at 2000 m. At 10 s, the velocity is 13.9 m/s at 1 m, increases to 24.0 m/s at 450 m, decreases to 13.4 m/s at 890 m, and then increases to 21.8 m/s at 1380 m. It is 11.2 m/s at 1820 m and 13.7 m/s at 2000 m.

The velocity with the Zhang model on a 2000 m circular road with $\beta = 0.1$ at 5 s, and 10 s is given in Fig. 14. This shows that the velocity exceeds the maximum of 30 m/s which is not realistic. At 5 s, the velocity is 21.6 m/s at 1 m, increases to 32.8 m/s at 290 m, decreases to 14.1 m/s at 600 m, and then increases to 29.8 m/s at 1250 m. It is 14.2 m/s at 1570 m and 21.2 m/s at 2000 m. At 10 s, the velocity is 21.1 m/s at 1 m, increases to 28.1 m/s at 350 m, decreases to 18.7 m/s at 780 m, and then increases to 25.8 m/s at 1300 m. It is 17.8 m/s at 1740 m and 20.9 m/s at 2000 m.

The velocity with the Zhang model on a 2000 m circular road with $\beta = 0.5$ at 5 s and 10 s is given in Fig. 15. This shows that again the maximum velocity of 30 m/s is exceeded. At 5 s, the velocity is 22.3 m/s at 1 m, increases to 33.4 m/s at 300 m, decreases to 12.3 m/s at 600 m, and then increases to 33.0 m/s at 1250 m. It is 12.7 m/s at 1570 m and 21.8 m/s at 2000 m. At 10 s, the velocity is 21.3 m/s at 1 m, increases to 29.5 m/s at 340 m, decreases to 18.0 m/s at 770 m, and then increases to 26.5 m/s at 1290 m. It is 17.3 m/s at 1750 m and 21.0 m/s at 2000 m.

The velocity with the Zhang model on a 2000 m circular road with $\beta = 1$ at 5 s and 10 s is shown in Fig. 16. The velocity now greatly exceeds the maximum of 30 m/s. At 5 s, the velocity is 22.8 m/s at 1 m, increases to 42.7 m/s at 310 m, decreases to 10.9 m/s at 640 m, and then increases to 36.5 m/s at 1260 m. It is 11.5 m/s at 1610 m and 22.2 m/s at 2000 m. At 10 s, the velocity is 21.3 m/s at 1 m, increases to 30.7 m/s at 340 m, decreases to 17.8 m/s at 800 m, and then increases to 26.9 m/s at 1290 m. It is 17.1 m/s at 1750 m and 21.1 m/s at 2000 m.

The velocity with the Zhang model on a 2000 m circular road with

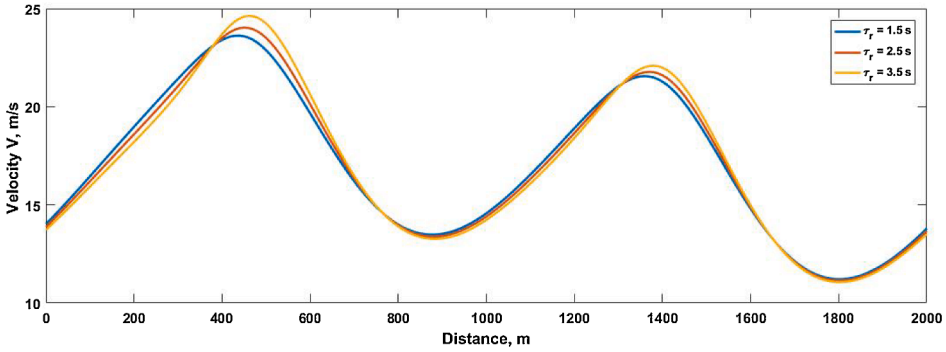

Fig. 4. Velocity with the KIG model on a 2000 m circular road with $h_f = h_r = 10$ m and $\tau_r = 1.5$ s, 2.5 s, and 3.5 s at 10 s.

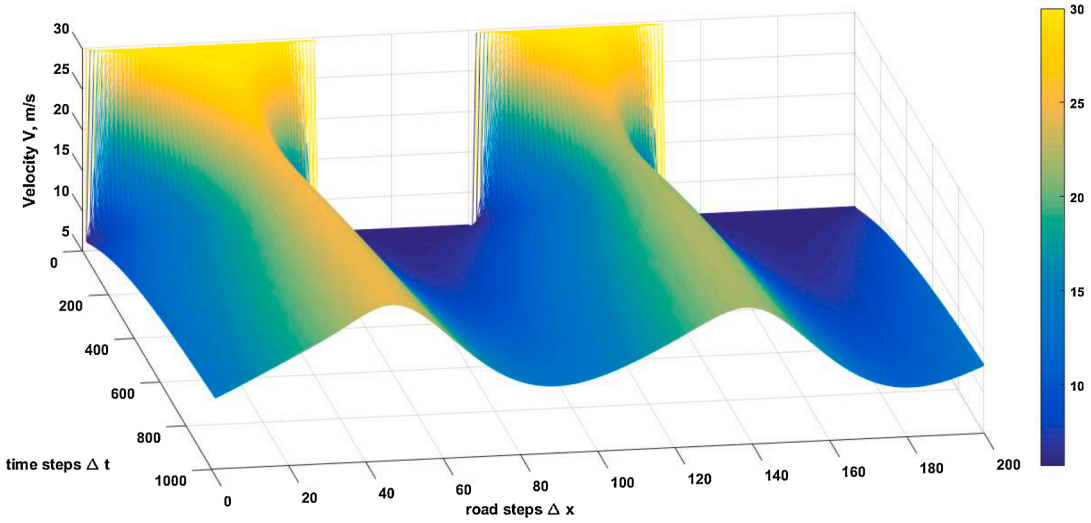

Fig. 5. Velocity with the KIG model on a 2000 m circular road with $h_f = h_r = 20$ m and $\tau_r = 1.5$ s for 10 s.

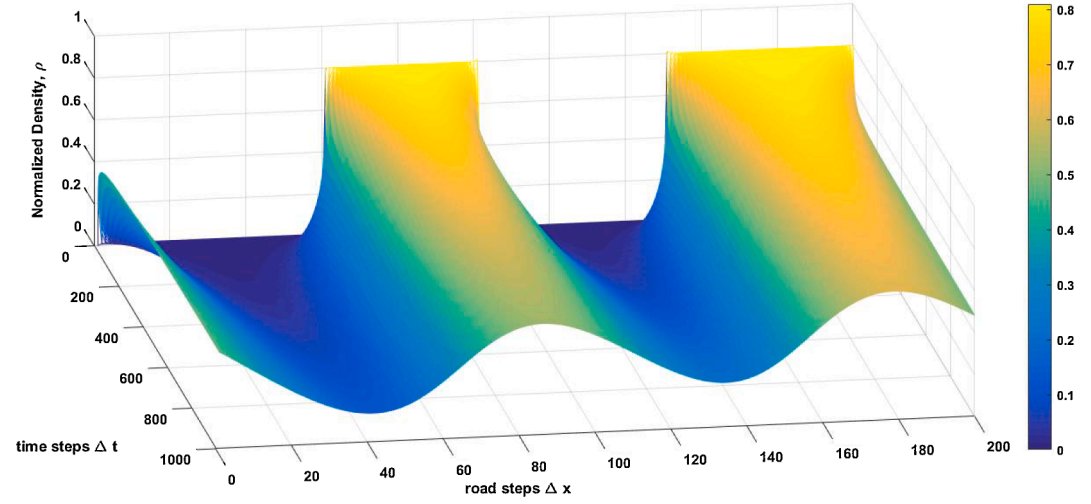

Fig. 6. Density with the KIG model on a 2000 m circular road with $h_f = h_r = 20$ m and $\tau_r = 1.5$ s for 10 s.

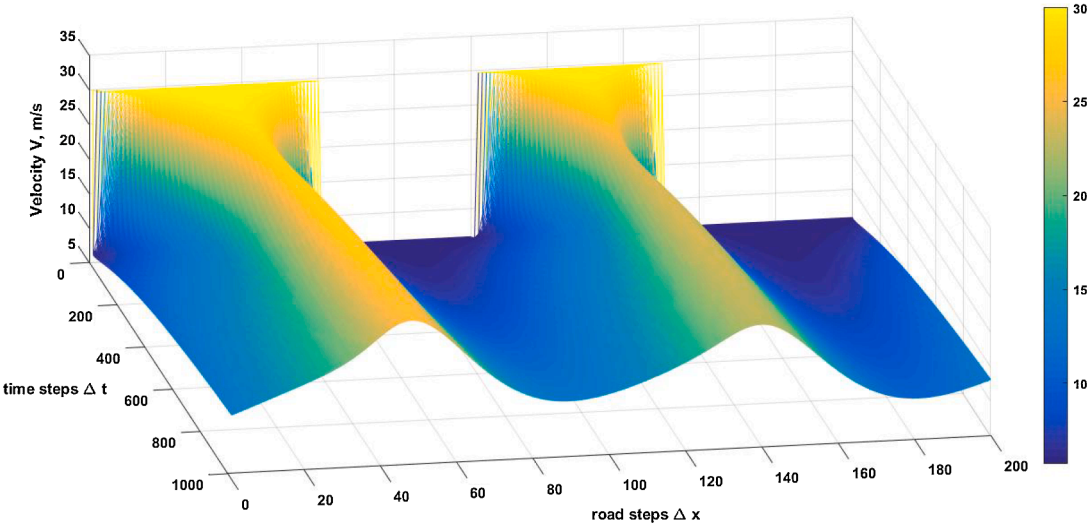

Fig. 7. Velocity with the KIG model on a 2000 m circular road with $h_f = h_r = 20$ m and $\tau_r = 2.5$ s for 10 s.

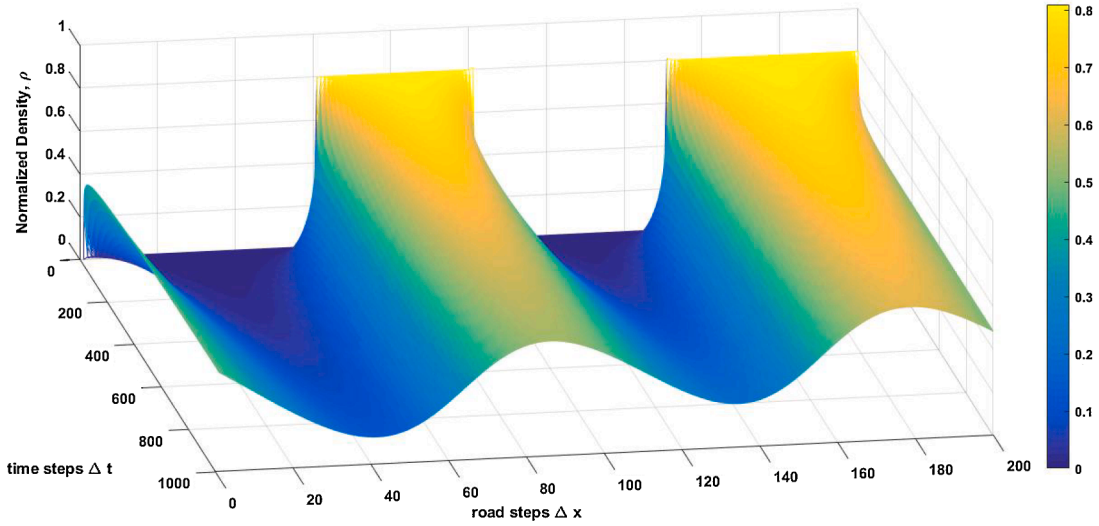

Fig. 8. Density with the KIG model on a 2000 m circular road with $h_f = h_r = 20$ m and $\tau_r = 2.5$ s for 10 s.

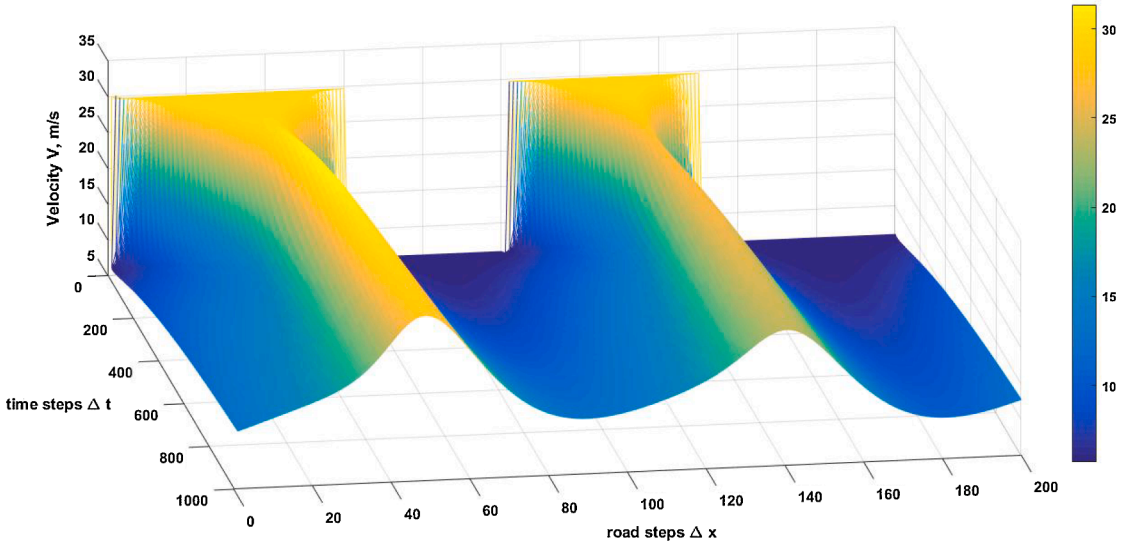

Fig. 9. Velocity with the KIG model on a 2000 m circular road with $h_f = h_r = 20$ m and $\tau_r = 3.5$ s for 10 s.

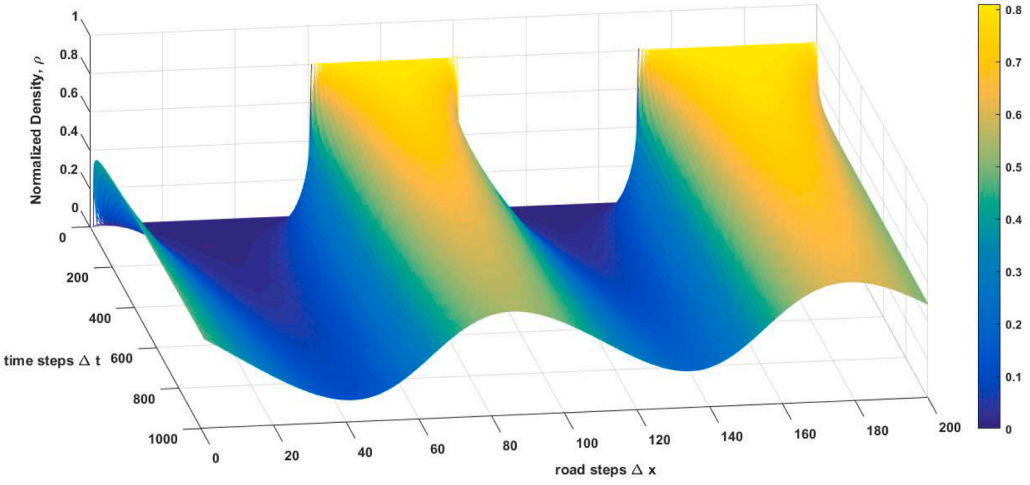

Fig. 10. Density with the KIG model on a 2000 m circular road with $h_f = h_r = 20$ m and $\tau_r = 3.5$ s for 10 s.

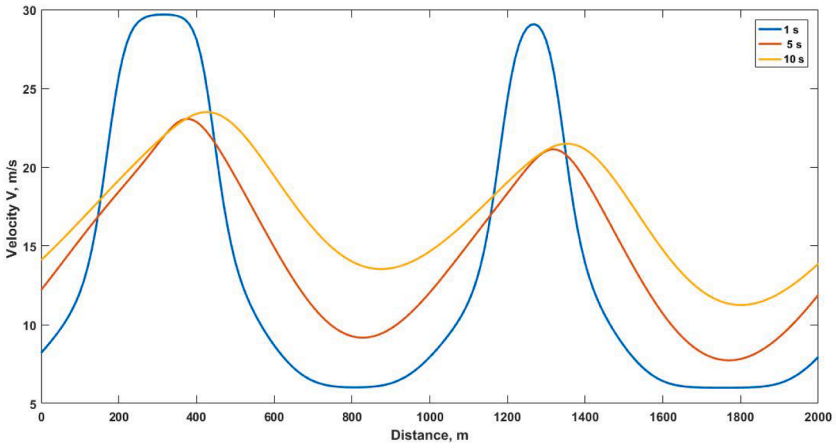

Fig. 11. Velocity with the KIG model on a 2000 m circular road with $h_f = 15$ m, $h_r = 12$ m, $\tau_r = 1.5$ s and $\beta = 0.6$ at 1 s, 5 s, and s 10 s.

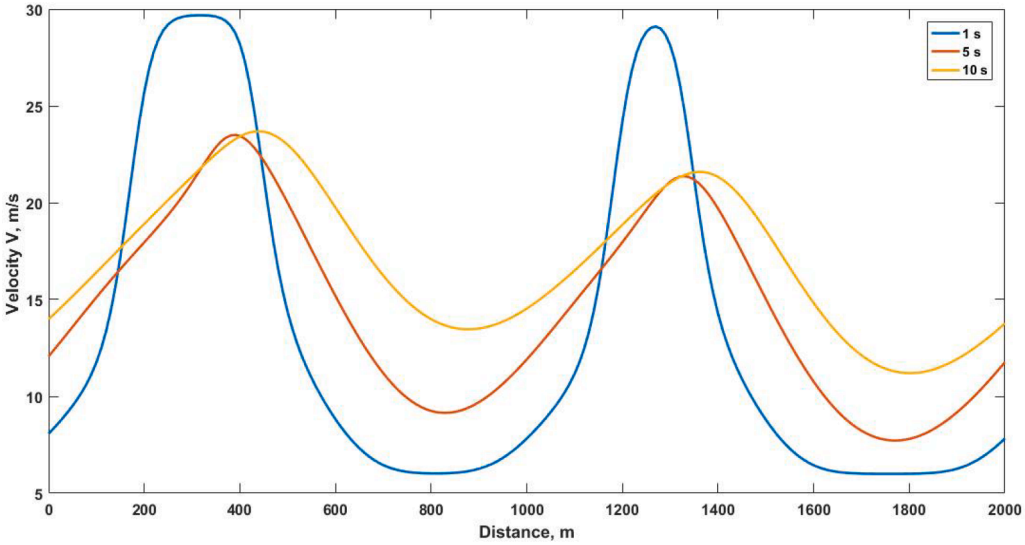

Fig. 12. Velocity with the KIG model on a 2000 m circular road with $h_f = 15$ m, $h_r = 12$ m, $\tau_r = 2.5$ s and $\beta = 1$ at 1 s, 5 s, and s 10 s.

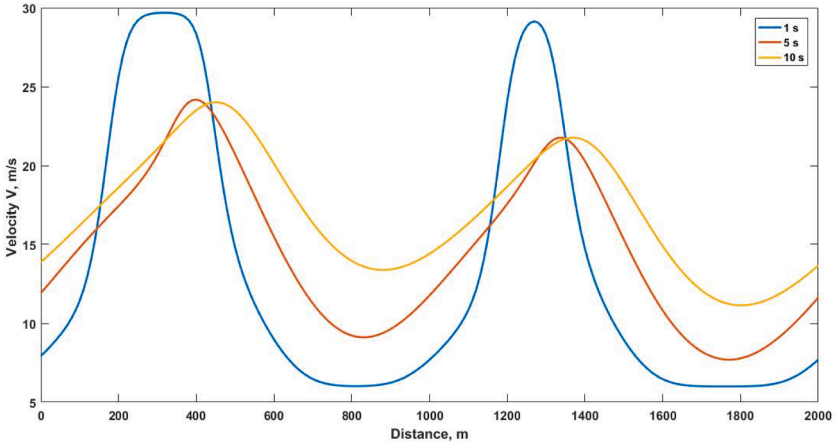

Fig. 13. Velocity with the KIG model on a 2000 m circular road with $h_f = 15$ m, $h_r = 12$ m, $\tau_r = 3.5$ s and $\beta = 1.4$ at 1 s, 5 s, and s 10 s.

$\beta = 0$ at 5 s and 10 s is shown in Fig. 17. The velocity again greatly exceeds the maximum of 30 m/s. At 5 s, the velocity is 26.2 m/s at 1 m, increases to 40.1 m/s at 260 m, decreases to 5.4 m/s at 550 m, and then increases to 35.4 m/s at 1210 m. It is 7.4 m/s at 1520 m and 25.6 m/s at 2000 m. At 10 s, the velocity is 23.7 m/s at 1 m, increases to 29.7 m/s at 280 m, decreases to 17.3 m/s at 730 m, and then increases to 26.1 m/s at 1720 m. It is 23.1 m/s at 2000 m.

The velocity with the Zhang model on a 2000 m circular road for 10 s

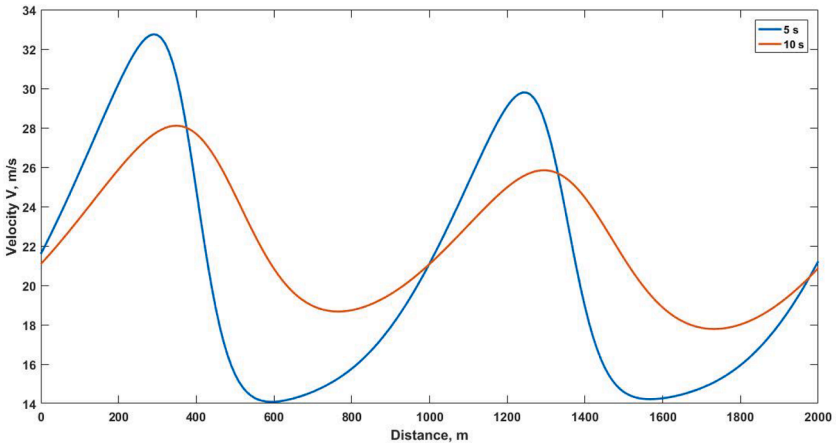

Fig. 14. Velocity with the Zhang model on a 2000 m circular road with $\beta = 0.1$ m at 5 s, and 10 s.

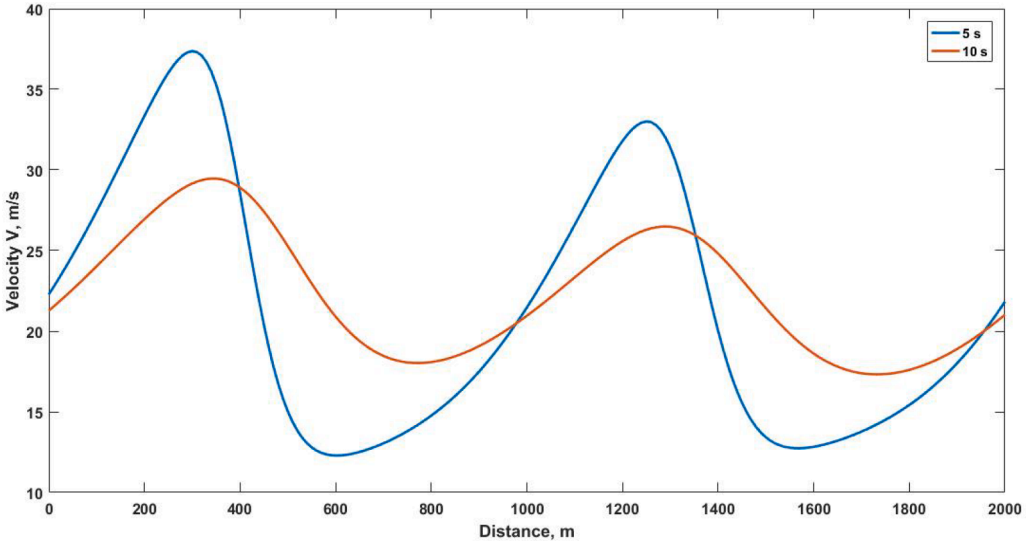

Fig. 15. Velocity with the Zhang model on a 2000 m circular road with $\beta = 0.5$ at 5 s and 10 s.

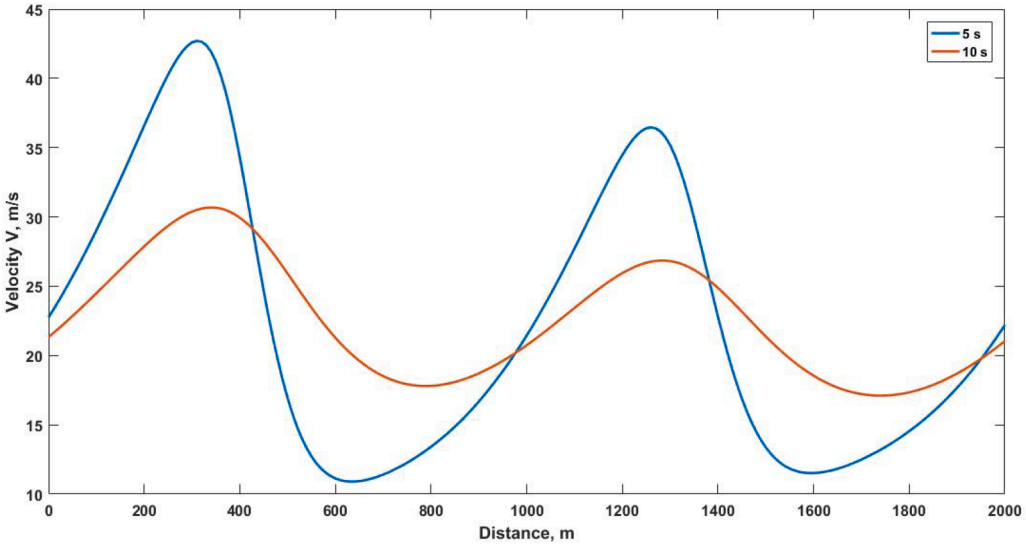

Fig. 16. Velocity with the Zhang model on a 2000 m circular road with $\beta = 1$ at 5 s and 10 s.

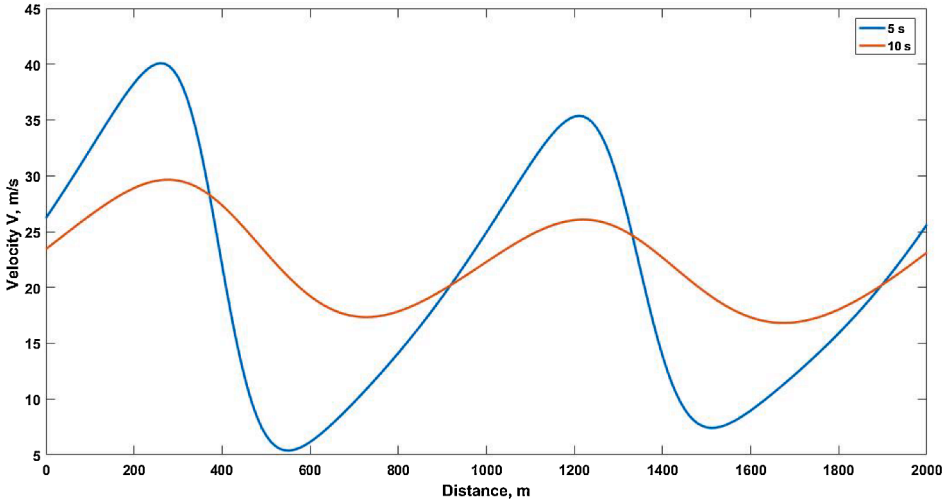

Fig. 17. Velocity with the Zhang model on a 2000 m circular road with $\beta = 0$ at 5 s and 10 s.

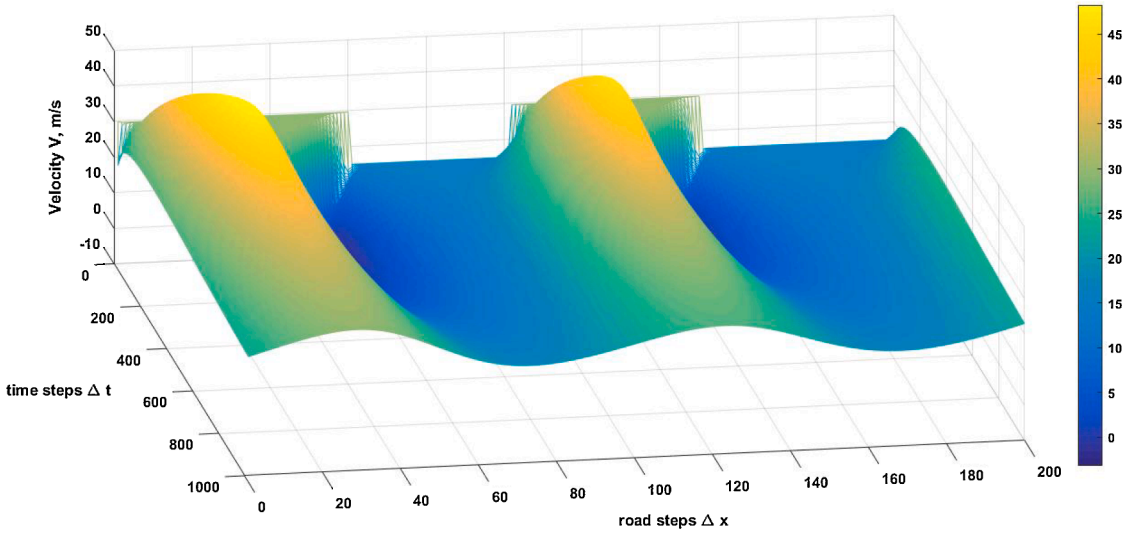

Fig. 18. Velocity with the Zhang model on a 2000 m circular road with $\beta = 0$ for 10 s.

with $\beta = 0$ is given in Fig. 18. This shows that the highest velocity is 47.6 m/s and the lowest is −3.1 m/s, which is impossible.

5.1. Discussion

The KIG model incorporates real traffic parameters such as h_r, h_r, τ and τ_f while the Zhang model does not explicitly consider these parameters. Thus, the Zhang model cannot be used to evaluate traffic flow under different conditions and driving behavior. The velocity and density evolution for both models was evaluated to determine if the output remains within the allowable range.

There are two important cases with the KIG model

$$\begin{cases} h_f = h_r & \text{uniform headway,} \\ h_f \neq h_r & \text{non-uniform headway.} \end{cases}$$

When $h_f = h_r = 20$ m (uniform headway) and $\tau_r = 1.5$ s, Fig. 1 shows that the velocity evolution is smooth and the velocity is always between the minimum and maximum values. With $\tau_r = 2.5$ s, Fig. 2 shows that the velocity evolution is very smooth as increasing τ_r increases β. Similarly, when τ_r is 3.5 s, the velocity behavior at 5 s and 10 s shown in Fig. 3 is smoother than with $\tau_r = 1.5$ s as in this case $\tau_r = \tau$ so $\beta = 1$. Figs. 5 and 6 give the velocity and density evolution of the KIG model, respectively, for 10 s with three values of τ_r. These results show that the model outputs are stable and stay within range.

When $h_f = 15$ m and $h_r = 12$ m (non-uniform headway) and $\tau_r = 1.5$ s, Fig. 11 shows that the velocity evolution is almost the same as with a uniform headway, but the average velocity is lower than in Fig. 1. The results for $\tau_r = 2.5$ s given in Fig. 12 show that the velocity behavior is similar to the uniform case in Fig. 2). However, Fig. 13 shows that as $\tau_r \rightarrow \tau$, driver memory approaches the maximum and the non-uniform headway results in significantly different velocity behavior than with a uniform headway as shown in Fig. 3.

The Zhang model performance was evaluated for $\beta = 0, 0.1, 0.5$, and 1. With $\beta = 0.1$, Fig. 14 shows that the velocity is 32.8 m/s at 5 s which exceeds the maximum velocity of 30 m/s. With $\beta = 0.5$, the maximum velocity is 33.4 m/s at 5 s and with $\beta = 1$, the maximum velocity is 42.7 m/s at 5 s. More problematic is that when $\beta = 0$, Fig. 18 shows that the velocity not only exceeds the maximum value, but is also −3.1 m/s which is impossible. Thus, it can be concluded that the Zhang model behavior due to large variations in density is not stable. This is because of the limitation of this model.

The results presented in this section clearly show that the velocity with the KIG model is more realistic than with the Zhang model. The velocity with the KIG model is within the allowable range for all values

of τ_r. Moreover, this model can provide results based on the driver memory β. Conversely, the Zhang model produces negative velocities with $\beta = 0$ and velocities above the maximum of 30 m/s for values between 0 and 1. Thus, the KIG model provides a better characterization of traffic.

6. Conclusion

A new traffic flow model was proposed to include traffic alignment behavior at transitions. The flow is characterized based on distance headway and driver memory whereas the Zhang model only considers driver memory. Results were presented which show that the proposed model provides realistic results based on the headway. The velocity evolves smoothly over time and stays within limits. On the other hand, the Zhang model produces large variations in velocity resulting in negative values and values that exceed the maximum.

Declaration of Competing Interest

We declare no conflict of interest.

Data availability

Some or all data, models, or code that support the findings of this study are available from the corresponding author upon reasonable request.

Acknowledgment

This Project was supported by the Higher Education Commission of Pakistan under the establishment of the National Center in Big Data and Cloud Computing at the University of Engineering and Technology, Peshawar.

References

[1] Z.H. Khan, W. Imran, T.A. Gulliver, K.S. Khattak, Z. Wadud, A.N. Khan, An anisotropic traffic model based on driver interaction, IEEE Access 8 (2020) 66799–66812.
[2] R. Jiang, Q. Wu, Z. Zhu, A new continuum model for traffic flow and numerical tests, Transp. Res. Part B Methodol. 36 (5) (2002) 405–419.
[3] Z.H. Khan, W. Imran, S. Azeem, K.S. Khattak, T.A. Gulliver, M.S. Aslam, A macroscopic traffic model based on driver reaction and traffic stimuli, Applied Sciences 9 (14) (2019).Art. 2848
[4] B. Kraft, Car Accidents Caused by Aggressive Driving, Kraft & Associates, 2023. [Online]. Available: https://www.kraftlaw.com/car-accidents/causes-car-accidents/car-accidents-caused-aggressive-driving/. [Accessed: 25-Apr-2023]
[5] G.M.H. Shahariar, T.A. Bodisco, A. Zare, M. Sajjad, M.I. Jahirul, T. Chu Van, H. Bartlett, Z. Ristovski, R.J. Brown, Impact of driving style and traffic condition on emissions and fuel consumption during real-world transient operation, Fuel 319 (2022).Art. 123874
[6] R.R. Knipling, M. Mironer, D.L. Hendricks, L. Tijeripa, J. Everson, J.C. Allen, C. Wilson, J.A. Volpe, Assessment of IVHS Countermeasures for Collision Avoidance: Rear-end Crashes. DOT HS 807 995 Final Report, US Department of Transportation, National Highway Traffic Safety Administration, 1993.
[7] M. Taieb-Maimon, D. Shinar, Minimum and comfortable driving headways: reality versus perception, Hum. Factors J. Hum. Factors Ergon. Soc. 43 (1) (2001) 159-172.
[8] W. Imran, Z.H. Khan, T.A. Gulliver, K.S. Khattak, H. Nasir, A macroscopic traffic model for heterogeneous flow, Chin. J. Phys. 63 (2020) 419–435.
[9] K. Nagel, P. Wagner, R. Woesler, Still flowing: approaches to traffic flow and traffic jam modeling, Oper. Res. 51 (5) (2003) 681–710.
[10] M. Lighthill, G. Whitham, On kinematic waves II. A theory of traffic flow on long crowded roads, Proc. R. Soc. London Ser. A Math. Phys. Sci. 229 (1178) (1955) 317–345.
[11] P. Richards, Shock waves on the highway, Oper. Res. 4 (1) (1956) 42–51.
[12] G. Liu, A. Lyrintzis, P. Michalopoulos, Improved high-order model for freeway traffic flow, Transp. Res. Record J. Transp. Res. Board 1644 (1) (1998) 37–46.
[13] C.F. Daganzo, Requiem for second-order fluid approximations of traffic flow, Transp. Res. Part B Methodol. 29 (4) (1995) 277–286.
[14] Z.H. Khan, T.A. Gulliver, A macroscopic traffic model for traffic flow harmonization, Eur. Transp. Res. Rev. 10 (2) (2018).Art. 30
[15] S. Maerivoet, B. De Moor, Transportation Planning and Traffic Flow Models, Katholieke Universiteit Leuven, Belgium, 2008.
[16] R. Ansorge, What does the entropy condition mean in traffic flow theory? Transp. Res. Part B Methodol. 24 (2) (1990) 133–143.
[17] H.J. Payne, Models of freeway traffic and control, Math. Models Public Syst. (Simulation Council Proceedings) 1 (1971) 51–61.
[18] H. Zhang, A theory of non-equilibrium traffic flow, Transp. Res. Part B Methodol. 32 (7) (1998) 485–498.
[19] G.B. Whitham, Linear and Nonlinear Waves, Wiley, New York, NY, USA, 1971.
[20] J.D. Castillo, P. Pintado, F. Benitez, The reaction time of drivers and the stability of traffic flow, Transp. Res. Part B Methodol. 28 (1) (1994) 35–60.
[21] W. Phillips, A kinetic model for traffic flow with continuum implications, Transp. Plann. Technol. 5 (3) (1979) 131–138.
[22] M. Grace, R. Potts, A theory of the diffusion of traffic platoons, Oper. Res. 12 (2) (1964) 255–275.
[23] E.F. Graham, D.C. Chenu, A study of unrestricted platoon movement of traffic, Traffic Eng. 32 (7) (1962) 11–13.
[24] M. Papageorgiou, Some remarks on macroscopic traffic flow modelling, Transp. Res. A 32 (5) (1998) 323–329.
[25] A. Aw, M. Rascle, Resurrection of second order" models of traffic flow, SIAM J. Appl. Math. 60 (3) (2000) 916–938.
[26] D.A. Richardson, Refined macroscopic traffic modelling via systems of conservation laws, Masters Thesis, 2012. Department of Mathematics and Statistics, University of Victoria, Victoria, BC, Canada.
[27] H. Zhang, Driver memory, traffic viscosity and a viscous vehicular traffic flow model, Transp. Res. Part B Methodol. 37 (1) (2003) 27–41.
[28] W. Imran, Z.H. Khan, T.A. Gulliver, M. Alam, K.S. Khattak, Non-homogeneous traffic characterization based on driver reaction and stimuli, Transp. Res. Interdiscip.Perspect. 21 (2023) 100858.
[29] W. Imran, L. Pariota, Macroscopic evaluation of traffic flow in view of connected and autonomous vehicles: a simulation-based approach, Alex. Eng. J. 79 (2023) 581–590.
[30] C. Zhai, W. Wu, A continuum model considering the uncertain velocity of preceding vehicles on gradient highways, Physica A 588 (2022).Art. 126561
[31] Y. Kang, S. Yang, A new anisotropic continuum traffic flow model with anticipation driving behavior. E3S Web of Conferences vol. 283, 2021.Art. 02036
[32] A. Nakayama, Y. Sugiyama, K. Hasebe, Effect of looking at the car that follows in an optimal velocity model of traffic flow, Phys. Rev. E 65 (1) (2002).Art. 016112
[33] H.X. Ge, H.B. Zhu, S.Q. Dai, Effect of looking backward on traffic flow in a cooperative driving car following model, Eur. Phys. J. B 54 (4) (2006) 503–507.
[34] D. Sun, The backward looking effect in lattice hydrodynamic model of pedestrian flow, J. Inf. Comput. Sci. 10 (7) (2013) 2067–2074.
[35] D.-H. Sun, X.-Y. Liao, G.H. Peng, Effect of looking backward on traffic flow in an extended multiple car-following model, Physica A 390 (4) (2011) 631–635.
[36] D. Yang, P. Jin, Y. Pu, B. Ran, Safe distance car-following model including backward-looking and its stability analysis, Eur. Phys. J. B 86 (3) (2013).Art. 92
[37] Z.H. Khan, T.A. Gulliver, A macroscopic traffic model based on transition velocities, J. Comput. Sci. 43 (2020).Art. 101131
[38] Z.H. Khan, T.A. Gulliver, A macroscopic traffic model based on anticipation, Arabian J. Sci. Eng. 44 (5) (2019) 5151–5163.
[39] J.V. Morgan. Numerical methods for macroscopic traffic models, Department of Mathematics, University of Reading, Berkshire, UK, 2002. Ph.D. Thesis.
[40] Z.H. Khan, T.A. Gulliver, W. Imran, K.S. Khattak, A macroscopic traffic model based on relaxation time, Alex. Eng. J. 61 (1) (2022) 585–596.
[41] D. Helbing, A. Johansson, On the controversy around Daganzo's requiem for and Aw-Rascle's resurrection of second-order traffic flow models, Eur. Phys. J. B 69 (2009) 549–562.
[42] M. Treiber, A. Kesting, Traffic Flow Dynamics: Data, Models and Simulation, Springer, Berlin, Germany, 2013.
[43] A. Jafaripournimchahi, et al., A viscous continuum traffic flow model based in the cooperative car following behavior of connected and autonomous vehicles, IET Intel. Transport Syst. (2022).
[44] A.K. Gupta, I. Dhiman, Analyses of a continuum traffic flow model for a nonlane-based system, Int. J. Mod. Phys. C 25 (10) (2014).Art. 1450045
[45] D. Ngoduy, C. Tampere, Macroscopic effects of reaction time on traffic flow characteristics, Phys. Scr. 80 (2) (2009).Art. 025802
[46] X. Chen, L. Li, Q. Shi, Empirical observations of stochastic and dynamic evolutions of traffic flow. Stochastic Evolutions of Dynamic Traffic Flow, 2015, pp. 27–47.
[47] C.A. de Moura, C.S. Kubrusly, The Courant-Friedrichs-Lewy (CFL) Condition: 80 Years After Its Discovery, Springer, Berlin, Germany, 2013.
[48] D. Khan, Z.H. Khan, W. Imran, K.S. Khattak, T.A. Gulliver, Macroscopic flow characterization at T-junctions, Transp. Res. Interdiscip. Perspect. 14 (2022) 100591.
[49] E.F. Toro, A. Hidalgo, M. Dumbser, Force schemes on unstructured meshes I: conservative hyperbolic systems, J. Comput. Phys. 228 (9) (2009) 3368–3389.
[50] P.P.E. Kachroo, S.A. Wadoo, S.J. Al-nasur, A. Shende, P.P.E. Kachroo, S.A. Wadoo, S.J. Al-nasur, Numerical methods, in: A. Shende (Ed.), Pedestrian Dynamics Feedback Control of Crowd Evacuation, Springer, New York, NY, USA, 2008, pp. 61–93.
[51] S. Islam, Z.H. Khan, T.A. Gulliver, K.S. Khattak, W. Imran, Pedestrian traffic characterization based on pedestrian response, IEEE Access 10 (2022) 118397–118408.
[52] Z.H. Khan, S.A.A. Shah, T.A. Gulliver, A macroscopic traffic model based on weather conditions, Chin. Phys. B 27 (7) (2018).Art. 070202
[53] D. Ni, Traffic Flow Theory, Elsevier, Amsterdam, Netherlands, 2016, pp. 55–58.
[54] N. Weik, Macroscopic traffic flow in railway systems–a discussion of the applicability of fundamental diagrams, J. Rail Transp. Plann. Manage. 23 (2002). Art. 100330

[55] L.E. Mararo, A macroscopic fundamental diagram for spatial analysis of traffic flow: a case study of Nyeri Town, Kenya, Am. J. Civil Eng. 3 (5) (2015) 150–156.
[56] C.F. Daganzo, N. Geroliminis, An analytical approximation for the macroscopic fundamental diagram of urban traffic, Transp. Res. Part B Methodol. 42 (9) (2008) 771–781.
[57] C.F. Daganzo, Y. Li, E.J. Gonzales, N. Geroliminis, City-scale transport modeling: an approach for Nairobi, Kenya. Institute of Transportation Studies, University of California Berkeley, Berkeley, CA, USA, 2007.
[58] P. Yi, J. Lu, Y. Zhang, H. Lu, Safety-based capacity analysis for chinese highways, IATSS Res. 28 (1) (2004) 47–55.
[59] K. Basak, et al., Modeling reaction time within a traffic simulation model. Proceedings of the International IEEE Conference on Intelligent Transportation Systems, 2013, pp. 302–309.The Hague, Netherlands